Water Self-Diffusion within Nematic Dispersions of Nanocomposites: A Multiscale Analysis of ^{1}H Pulsed Gradient Spin−Echo NMR Measurements

P. Porion, M. Al Mukhtar, A. M. Faugère, R. J. M. Pellenq, S. Meyer, and A. Delville*

CRMD, CNRS, 1b rue de la Férollerie, 45071 Orléans Cedex 02, France

Received: September 27, 2002; In Final Form: February 4, 2003

We have used a multiscale statistical analysis to interpret the mobility of water molecules diffusing within nematic aqueous dispersions of charged anisotropic nanocomposites (synthetic Laponite clays). The nematic ordering of dense aqueous suspensions (29−52% w/w) prepared by uniaxial compression is detected by analyzing the splitting of the nuclear magnetic resonance line of the quadrupolar counterions (^{7}Li and ^{23}Na) neutralizing the negative charges of the clay. The tensor describing the water self-diffusion is measured by ^{1}H pulsed gradient spin−echo (PGSE) NMR spectroscopy. It exhibits a large anisotropy of water mobility in these nematic dispersions. The macroscopic mobility of the water molecules is obtained from numerical simulations of Brownian dynamics (BD), by integrating the water trajectories over a time scale of 1 μs. The local mobility of the water molecules in the vicinity of the surface of the Laponite particles is deduced from preliminary molecular dynamics (MD) simulations of the trajectories of the water molecules confined between two clay fragments by integrating their trajectories over a time scale of a few picoseconds. The equilibrium density and initial configuration of these confined water molecules are deduced from grand canonical Monte Carlo (GCMC) simulations, by using a new clay/water force field determined from semi-empirical periodic (MINDO) quantum calculations coupled to perturbation theory for dispersion forces. This multiscale statistical analysis of the water mobility bridges the gap between the time scale (nanoseconds) accessible by MD simulations and the time scale (microseconds) accessible by BD, leading to macroscopic behavior comparable with experimental data.

(I) Introduction

Clays are charged anisotropic colloids used in many industrial applications (waste management and storage, heterogeneous catalysis, drilling, ionic exchange, etc.) exploiting their various physico-chemical properties (large affinity for water molecules and polar solvents, high specific surface and surface charge density, gelling, thixotropy, surface acidity, etc.). By contrast with natural clays which contains numerous impurities, Laponite is a synthetic clay frequently used for scientific investigations[1−13] because of its high chemical purity. Thus we have used this synthetic clay in order to validate our experimental procedures before investigating the behavior of the natural clay materials which are used for the industrial applications. Laponite clay results from the sandwiching of one layer of magnesium oxides, with an octahedral geometry, between two layers of silicium oxides, with an tetrahedral geometry. In dilute aqueous regime, Laponite clays behave as isolated rigid disks (diameter, 200−300 Å; thickness, 10 Å; and density, 2.7).[8,14,15] Because of the substitution of some Mg^{2+} cations from their octahedral network by Li^+ cations, each Laponite disk bears about a thousand of negative electric charges neutralized by hydrated sodium counterions.

The purpose of this study is to determine the mobility of the water molecules in the vicinity of clay surfaces because this parameter is crucial for monitoring and understanding its use for storage applications.[16] Pulsed gradient spin−echo (PGSE) NMR spectroscopy is a powerful tool to derive this information at a macroscopic scale.[17,18] The challenge resides in the way of relating this macroscopic information, such as the macroscopic self-diffusion coefficient, to the local mobility of the solvent molecules and its interaction with the clay surface. This micro/macro transition is performed by a multiscale modeling of aqueous clay dispersions, bridging the length gap between 1 Å and 1 μm and the time gap between 1 ps and 1 μs. For that purpose we have used complementary quantum and statistical tools. First the interaction between one water molecule and a small clay fragment (8.97 × 10.36 Å^2) is evaluated from periodic (MINDO) calculations for a large set of configurations of the water molecule. The electric charge and polarizability of the atoms from the clay network and the soft short-range clay/water repulsion are deduced from this quantum study. Clay/water dispersion interactions are calculated from atomic polarizabilities following the PN-TrAZ model,[32,33] and used to describe the clay/water and ion/water force field compatible with empirical atomic models of the interactions between the water molecules (TIP4P) and the sodium counterions. Grand canonical Monte Carlo (GCMC) simulations[19,20] are then performed with a larger clay fragment (35.88 × 31.08 Å^2) to determine the equilibrium density and some configurations of the water molecules in equilibrium with bulk water and confined between two Laponite particles with a period of 30 Å. Molecular dynamics (MD) simulations[21,22] are then performed in the same simulation cell, integrating the water trajectories during 250 ps with a time step of 1 fs. The three eigenvalues of the tensor describing the local mobility of these confined water molecules are evaluated during these MD simulations, by integrating the three components of the water velocity autocorrelation function. This local mobility is then used for Brownian dynamics (BD) simulations[23] to analyze the trajectories of 10000 water mol-

10.1021/jp022161q CCC: $25.00
Published on Web 04/04/2003

ecules diffusing through a large set of rigid disks mimicking Laponite clay particles. The width of this last simulation cell is 0.14 μm, and the water trajectories are integrated over 1 μs with a time step of 20 ps. The water mobility within the porous network limited by these solid/liquid interfaces is further analyzed during these BD simulations by calculating the water self-diffusion propagator,[18] whose Fourier transform is directly comparable to ^{1}H PGSE NMR experimental data.[17,18]

These complementary quantum (MINDO) and statistical (GCMC, BD, and MD) approaches allow us to derive, from molecular orbital quantum calculations of the clay/water interaction, the macroscopic mobility of the water molecules within aqueous clay dispersions by avoiding, as much as possible, the use of empirical parameters. Many numerical studies[24−27,60,61] have been devoted to this problem, but to our knowledge, this self-consistent approach is performed for the first time.

(II) Materials and Methods

(A) Sample Preparation. Sodium Laponite RD from Laporte (general formula per unit cell: $Si_8Mg_{5.3}Li_{0.7}O_{24}H_4Na_{0.7}$) is used without purification. It is dispersed in water at pH 10, by NaOH addition, to avoid the acidic dissolution of magnesium oxide from the octahedral network.[28,29] The exchange of the solvated sodium counterions by lithium was performed first by dispersing the clay particles within LiCl 10^{-1} M and LiOH 10^{-4} M aqueous solutions during at least one week to obtain dilute clay dispersions (3% w/w). The clay particles are then extracted by centrifugation (20 min at 15000 rev/min), and the full procedure is repeated five times. Finally, the clay fraction is dispersed in LiOH 10^{-4} M solutions and dialyzed under N_2 against LiOH 10^{-4} M solutions during at least 1 month to remove excess lithium counterions. We have used a dialysis bag with a small pore size (molecular weight cutoff 1000 from Spectra) to minimize the release of Laponite particles. Concentrated samples are prepared by oedometric uniaxial compressions of dilute samples (5% w/w) by using external pressures varying between (4.6 and 11.6) $\times$ 10^5 Pa, leading to Laponite concentrations varying between 29 and 52% (w/w). Here also the pore size of the membrane (0.1 μm from Osmonics) is selected to minimize the release of clay particles. At least 1 month is required to consolidate these dense clay samples. The final clay density is evaluated by measuring its water loss at 80 °C under vacuum.

(B) NMR Experiments. ^{23}Na and ^{7}Li NMR spectra were recorded on a DSX 360 Bruker spectrometer, with a static field of 8.465 T. A broad spectral width (1 MHz) and a fast acquisition procedure (time step 1 μs) were used to record the ^{23}Na spectra in the presence of clay. ^{7}Li spectra were recorded with a smaller spectral width (250 kHz) with a fast acquisition procedure (time step 4 μs). Typical pulse durations necessary to tilt the magnetization in the transverse detection plane were equal to 14 and 7.5 μs for ^{23}Na and ^{7}Li, respectively. The analysis of the spectra of these $^3/_2$ spin nuclei presenting a residual static quadrupolar coupling is performed, as previously,[30] by a numerical simulation of the time evolution of the different coherences during each elementary step of the RF pulse [π/2 pulse−τ delay−acquisition, where τ (4.5 μs) is the irreducible time delay of our spectrometer]. This procedure is necessary to reproduce the depletion of the resonance line near to the central line of the triplet (see Figure 1) because of the coherence relaxation which mixes, even during a single RF pulse, the one-quantum coherences of all ranks.[30]

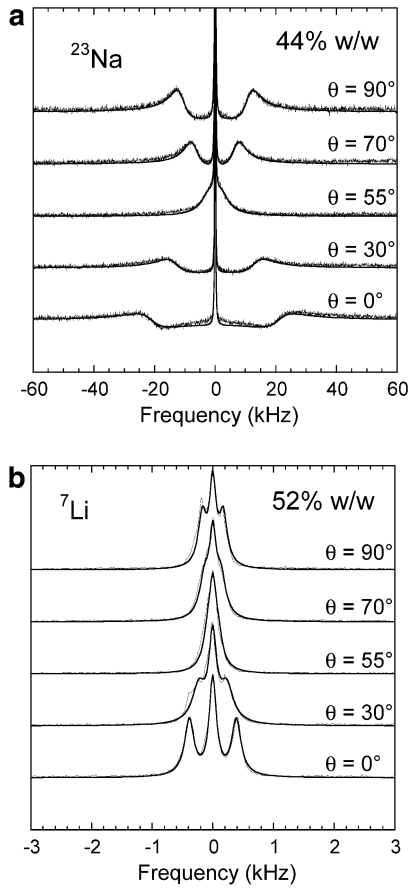

Figure 1. Angular variation of the splitting of the nuclear magnetic resonance line of quadrupolar nuclei in the presence of dense Laponite dispersions: (a) ^{23}Na spectra (44% w/w) and (b) ^{7}Li spectra (52% w/w).

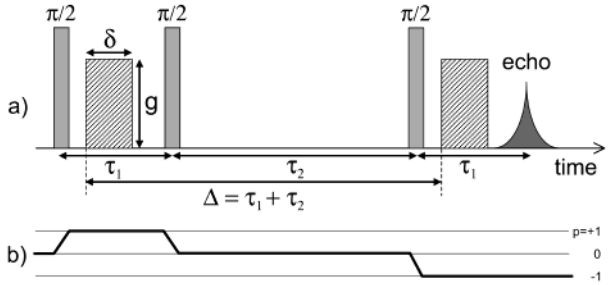

Figure 2. (a) Stimulated echo pulse sequence used for the measurement of the water self-diffusion. The three 90° pulses produce a stimulated spin−echo at $2\tau_1 + \tau_2$. Between the second and third pulse, the magnetization is locked along the static magnetic field during the time τ_2. The diffusion time is $\Delta = \tau_1 + \tau_2$. (b) Coherence transfer pathway ($p = 0 \rightarrow +1 \rightarrow 0 \rightarrow -1$) resulting from an adequate phase cycling.

^{1}H pulsed gradient spin−echo (PGSE) NMR is used to determine the macroscopic mobility of the water molecules along the three principal directors of the diffusion tensor within the dense nematic Laponite dispersions. We measure the decrease of the ^{1}H intensity as a function of increasing magnetic field gradient. The diffusion weighted stimulated echo pulse sequence has been used (see Figure 2) with an echo attenuation[17,18] according to

$$\frac{I(q)}{I(0)} = \exp[-4\pi^2 q^2 \vec{e}_g^{\,T} \overleftrightarrow{D} \vec{e}_g (\Delta - \delta/3)] \qquad (1)$$

where $q = \gamma g \delta / 2\pi$, g is the intensity of the applied field gradient (varying between 0 and 1.2 T/m), $\vec{e}_g$ its direction, δ its duration, Δ the diffusion time, γ the gyromagnetic ratio of the nuclei, $\overleftrightarrow{D}$

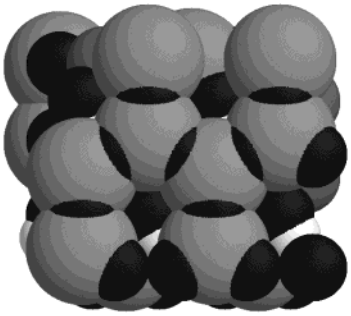

Figure 3. Fragment of Montmorillonite clay used for the MINDO calculations.

the self-diffusion tensor, and $I(q)$ and $I(0)$ the echo intensities, respectively, measured with and without the field gradient. Since the same pulse sequence, using the same coherence pathway, is used for recording the echo intensities with $I(q)$ and without $I(0)$ field gradients, they are both affected by the relaxation mechanisms of the water molecule, leading to the same echo attenuation $[I(0) \sim \exp(-2\tau_1/T_2)\exp(-\tau_2/T_1)]$. As a consequence, the water relaxation mechanisms do not contribute to the measured ratio $I(q)/I(0)$. The maximum value of the magnetic field gradient (1.2 T/m) corresponds to wavenumbers q smaller than 51×10^3 m^{-1}. The diffusion measurements are thus macroscopic and result from averages over a sample size larger than 20 μm. The samples are macroscopic cylinders (thickness, 4 mm; diameter, 4 mm) cut into the dense aqueous dispersions of clay. The diffusion experiments were performed on a Bruker DSX 100 spectrometer equipped with a microimaging probe (Micro5 Bruker) with gradient coils in three perpendicular directions used to generate magnetic field gradients along any arbitrary direction $\vec{e}_g$. The temperature was fixed at 296 K.

(C) Numerical Simulations. *(1) Derivation of the Atomic Clay/Water Potential*. MINDO quantum calculations were first performed for a single water molecule in the presence of two unit cells of an ideal Montmorillonite clay (general formula per unit cell: $Si_8Al_4O_{24}H_4$)(see Figure 3) for a large set (1833) of configurations of the water molecule. A typical energy profile of the clay/water soft core repulsion is illustrated in Figure 4. By contrast with our previous[31] MINDO calculations, this MINDO program (MOPAC 93 from Fujitsu) uses block atomic waves functions whose periodicity greatly improves the reliability of the results by suppressing the use of dangling bonds.[31] Mulliken population analysis was used to determine the atomic charges of the clay network. The energy of the 1833 configurations of the clay/water supermolecule was fitted on a simple analytical expression, and the q_j, b_{ij}, D_{ij}, A_{ij}, and C_{ij} parameters are detailed in Tables 1 and 2

$$E_{\text{el+rep}} = \sum_{i=1}^{N_{\text{wat}}}\sum_{j=1}^{N_{\text{at}}}\left[\frac{q_i q_j}{4\pi\epsilon_0 r_{ij}} + D_{ij}\exp(-b_{ij}r_{ij}) + \frac{A_{ij}}{r_{ij}^2}\right] \quad (2)$$

where N_{wat} stands for the oxygen and hydrogen atoms of the water molecule and N_{at} those of the clay fragment. As shown in Table 2, the coefficient $A_{i\text{O}}$ and $A_{i\text{H}}$ of eq 2 are selected, as previously,[31] in order to compensate each other ($A_{i\text{H}} = -0.5A_{i\text{O}}$) where the index i stands for each type of atoms from the clay network. As a consequence, the long-distance behavior of that contribution to the clay/water potential evolves according to r^{-3}, ensuring its convergence. Because of the large size of our GCMC simulation cell, no correction is introduced to compensate for the cutoff of this negligible long-distance contribution. The geometry and the atomic charges of the water molecules were those of the TIP4P water model ($q_{\text{O}} = 1.04e$).

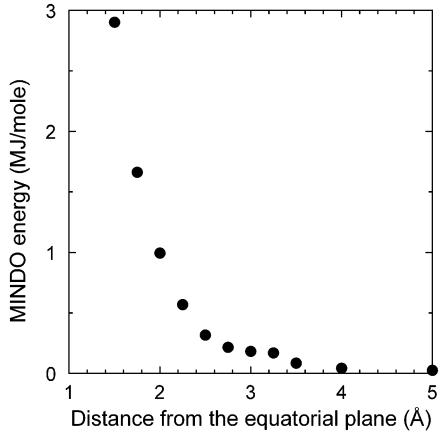

Figure 4. Variation of the MINDO quantum energy of the clay/water supramolecule as a function of the distance of the water oxygen atom from the octahedral layer of the clay.

TABLE 1: Partial Atomic Charges Obtained from the Quantum Calculation[a]

Si	$-2.67e$
Al	$-2.12e$
O_1	$1.36e$
O_2	$0.95e$
H	$-0.29e$

[a] The O_2 molecules are located at the center of the hexagonal cavity (four per unit cell; see Figure 3).

TABLE 2: Parameters Describing the Clay/Water Potential

	Si	Mg	O_1	O_2	H
$b_{i,\text{Ow}}$ (Å^{-1})	4.83	4.83	3.32	3.32	2.45
$b_{i,\text{Hw}}$ (Å^{-1})	8.77	8.77	2.45	2.45	5.26
$D_{i,\text{Ow}}$ (MJ/mol)	417	417	75	75	7.2
$D_{i,\text{Hw}}$ (MJ/mol)	10.	10.	7.2	7.2	200
$A_{i,\text{Ow}}$ [MJ/(Å^2 mol)]	.058	.058	−0.08	−0.08	0.04
$A_{i,\text{Hw}}$ [MJ/(Å^2 mol)]	−0.029	−0.029	0.04	0.04	−0.02
$C_{i,\text{Ow}}$ [MJ/(Å^6 mol)]	0.681	0.	2.53	2.12	0.40
$C_{i,\text{Hw}}$ [MJ/(Å^6 mol)]	0.135	0.	0.477	0.396	0.083

MINDO calculations being an approximation of the self-consistent Hartree−Fock approach, they do not include dispersion interactions. The clay/water dispersion interaction is calculated in a self-consistent manner from the atomic polarizabilities estimated on the basis of the net atomic charges of the water molecules and the clay particle. According to the PN-TrAZ procedure,[32,33] this description of the dispersion contribution matches the soft-core repulsion evaluated from our quantum calculations since it is based on a description including damping functions parametrized with the repulsive parameters ("b_{ij}" in eq 2) fitted from MINDO results:

$$E_{\text{disp}} = -\sum_{i=1}^{N_{\text{wat}}}\sum_{j=1}^{N_{\text{at}}}\frac{C_{ij}}{r_{ij}^6}\left[1 - \left(\sum_{k=0}^{6}\frac{(b_{ij}r_{ij})^k}{k!}\right)\exp(-b_{ij}r_{ij})\right] \quad (3)$$

This approach, which allows for a good degree of transferability, was successfully used to describe rare gas, xylene, and water adsorption in various zeolites, silicon porous materials, and at the surface of metal oxydes.[32,33,57] The clay/sodium potential were derived in the same manner by focusing on the leading contributions from the oxygen atoms of the clay network. The parameters are detailed in Table 3. In addition to these clay/

TABLE 3: Parameters Describing the Clay/Sodium Potential

	Si	Mg	O_1	O_2	H
$b_{i,Na}$ (Å^{-1})	3.33	3.33	3.33	3.33	3.33
$D_{i,Na}$ (MJ/mol)	90.	90.	90.	90.	90.
$C_{i,Na}$ [MJ/(Å^6 mol)]	0.125	0.	0.457	0.389	0.063

water and clay/sodium potentials, an empirical TIP4P potential[34] was used to describe the water/water interaction. The water/water pair potential is described as the sum of the electrostatic contributions evaluated between the nine pairs of charged centers and the oxygen/oxygen van der Waals interaction given by the empirical relation

$$E_{vdw} = \frac{A_{OO}}{r^{12}} - \frac{B_{OO}}{r^6} \tag{4}$$

with $A_{OO} = 2.511208 \times 10^6$ Å^{12} kJ/mol and $B_{OO} = 2.55395 \times 10^3$ Å^6 kJ/mol. The Na^+/water potential[35] is compatible with the TIP4P potential; it results from the sum of a three-center electrostatic interaction and a van der Waals interaction between the Na^+ ion and the atoms of the water molecule. The Na^+/oxygen short-range interaction is given by

$$E_{short} = A_{NaO} \exp(-b_{NaO} r) - \frac{C_{NaO}}{r^4} - \frac{D_{NaO}}{r^6} \tag{5a}$$

with $A_{NaO} = 1.144 \times 10^5$ kJ/mol, $b_{NaO} = 3.5455$ Å^{-1}, $C_{NaO} = 1.820 \times 10^3$ Å^4 kJ/mol, and $D_{NaO} = -3.515 \times 10^3$ Å^6 kJ/mol. The Na^+/hydrogen soft-core repulsion is given by

$$E_{short} = A_{NaH} \exp(-b_{NaH} r) \tag{5b}$$

with $A_{NaH} = 8.612 \times 10^3$ kJ/mol and $b_{NaH} = 3.3940$ Å^{-1}. This new model of clay hydration is more consistent than our previous one,[31] since the same atomic charges of the water molecules are used to describe the water/water, the water/ion, as well as the clay/water interactions.

(2) Grand Canonical Monte Carlo Simulations. The simulation cell used in these Monte Carlo simulations results from the stack of three clay sheets, each composed from 24 unit cells of Laponite and each neutralized by 16 sodium counterions. The period of the stack is 30 Å and the size of the whole simulation cell is $35.88 \times 31.08 \times 90$ Å^3. A period of 30 Å was selected since the clay/water interface was shown to modify the thermodynamical properties of water[38,39,58,59] over a deepness of only 10 Å, corresponding roughly to three hydration layers. As a consequence, at separation larger than 15 Å from the equatorial plane of the clay, the well-known thermodynamical properties of bulk water are recovered. In this modeling of Laponite hydration we used the same parameters as those derived to describe the interactions of the Na^+ ions and the water molecules with Montmorillonite clay (see section II.C.1). The atomic charge of the octahedral Mg ions is evaluated from the atomic charges of an ideal Montmorillonite clay (see section II.C.1) as detailed in Table 1, and selected in order to ensure the electroneutrality of an ideal model of Laponite clay (general formula per unit cell: $Si_8Mg_6H_4O_{24}$). Sixteen substitutions of the octahedral Mg atoms by Li atoms are generated randomly within each clay sheet.

Periodic boundary conditions are applied in all directions and Ewald summation[36] is used to derive the long-range contribution of the electrostatic energy cut by minimum image approximation

$$E_{elect} = E_{dir} + E_{rec} + E_{mom} + E_{self} \tag{6a}$$

$$E_{dir} = \frac{1}{8\pi\epsilon_0\epsilon_r} \sum_{i=1}^{N_i} q_i \sum_{j=1, i\neq j}^{N_j} \frac{q_j erfc(\kappa r_{ij})}{r_{ij}} \tag{6b}$$

$$E_{rec} = \frac{1}{2V\epsilon_0\epsilon_r} \sum_{K,|K|\neq 0} \frac{\exp(-|\vec{K}|^2/4\kappa^2)}{|\vec{K}|^2} [\{\sum_i q_i \cos(\vec{K}\times\vec{r}_i)\}^2 + \{\sum_j q_j \sin(\vec{K}\times\vec{r}_j)\}^2] \tag{6c}$$

$$E_{mom} = \frac{1}{2V(1+2\epsilon_\infty)\epsilon_0\epsilon_r} (\sum_{i=1} q_i \vec{r}_i)^2 \tag{6d}$$

$$E_{self} = \frac{-\kappa}{4\pi^{3/2}\epsilon_0\epsilon_r} \sum_i q_i^2 - \frac{1}{8\pi\epsilon_0\epsilon_r} \sum_{\alpha=1}^{n_\alpha} \sum_{i=1} q_i \sum_{j=1, j\neq i}^{n_\alpha} \frac{q_j erf(\kappa r_{ij,\alpha})}{r_{ij,\alpha}} \tag{6e}$$

where the second term of eq 6e is evaluated for every set of electric charges pertaining to the same water molecule or clay sheet. The effective dielectric constants of eq 6a−e are $\epsilon_r = 1$ and $\epsilon_\infty = 80$. Exactly 2196 replications where used for the summation over the reciprocal space, and the damping parameter κ wass set equal to 0.19 Å^{-1} leading to an accuracy of the Ewald procedure[37] better than 0.002.

We selected to sample the grand canonical ensemble,

$$\Xi(\mu,V,T) = \sum_{N_w} \left(\frac{V}{\lambda_w^3}\right)^{N_w} \frac{\exp(\beta N_w \mu)}{N_w!} \int\ldots\int \exp(-\beta E) d\vec{\tau}_1 \ldots d\vec{\tau}_N \tag{7}$$

to simulate at 298 K the confined water molecules in equilibrium with bulk water (whose chemical potential is μ). The GCMC procedure is also very useful to determine the density of the confined water molecules[31,38] and predict adsorption isotherms.[39]

We used block averages with more than 10000 blocks of 50000 iterations to thermalize the initial configuration and twice that value to average the data. The block size was at least 10 times larger than the total number of water molecules in the simulation cell (~2400 at equilibrium). At each step of the GCMC procedure[19,20] we selected randomly, with an equal probability, either to displace randomly a sodium cation (translation) or a water molecule (translation plus rotation) inside their own layer, or to add randomly a water molecule, or to remove a randomly selected water molecule. According to the Metropolis procedure generalized to sample the grand canonical ensemble, the acceptance ratios satisfy

$$P_{deplac} = \min[1, \exp(-\beta\Delta E)] \qquad \text{for the displacements} \tag{8a}$$

$$P_{add} = \min\left[1, \frac{\exp(B)\exp(-\beta\Delta E)}{N_w + 1}\right] \qquad \text{for adding one water molecule} \tag{8b}$$

$$P_{rem} = \min\left[1, \frac{N_w \exp(-\beta\Delta E)}{\exp(B)}\right] \qquad \text{for removing one water molecule} \tag{8c}$$

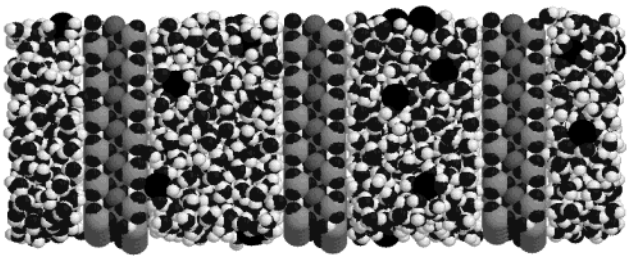

Figure 5. Snapshot of one equilibrium configuration of the water molecules and sodium counterions confined between three Laponite particles with a period of 30 Å.

where $B = \beta\mu + \ln(V/\lambda_w^3)$. The initial configuration of a reduced number of confined water molecules ($\sim$10) and of the 48 sodium counterions is generated randomly, each layer being electrically neutral. Figure 5 displays a snapshot of one equilibrium configurations of these confined water molecules and sodium counterions.

(3) Molecular Dynamics Simulations. After thermalization of the GCMC simulations, we selected one of the three stacks of water molecules and 16 sodium counterions confined between two clay sheets (cf. Figure 5) and simulated their trajectories by using the Verlet algorithm.[21] During these MD simulations, the clay particles and the water molecules were assumed to remain rigid. The quaternion procedure was used to describe water rotation in the framework of a generalized Verlet algorithm.[21,22,40] A Berendsen thermostat[41] was applied to each component of the translational $E_{transl}(3)$ and rotational $E_{rot}(3)$ kinetic energy. As a consequence, each component of the water or ionic velocities is multiplied by the factor

$$x_{transl}(i) = \sqrt{1 + \xi\left(\frac{T - E_{transl}(i)}{E_{transl}(i)}\right)} \qquad (9a)$$

and each component of the water angular velocity is multiplied by the factor

$$x_{rot}(i) = \sqrt{1 + \xi\left(\frac{T - E_{rot}(i)}{E_{rot}(i)}\right)} \qquad (9b)$$

Weak coupling with the thermostat ($T = 298$ K) is ensured by setting the parameter $\xi = 0.33$. An elementary time step of 1 fs is used to integrate the trajectories of the water molecules and 0.1 fs for that of the ions. The average temperature corresponding to each motion was stabilized at 298 $\pm$ 5 K during 250 ps. To evaluate the statistical errors on the different autocorrelation functions, the whole trajectory is cut into 50 independent sections, assuming no correlation propagates on a time scale larger than 5 ps.

The mobility of diffusing species is generally evaluated from the asymptotic behavior of the mean-square displacement of the probe

$$D_\alpha = \lim_{\tau\to\infty} \sum_{i=1}^{N_{wat}} \frac{(x_{i,\alpha}(0) - x_{i,\alpha}(\tau))^2}{2N_{wat}\tau} \qquad (10)$$

However, since the motion of the confined water molecules and solvated counterions is limited in the transverse direction (perpendicular to the clay surface), the asymptotic value estimated by eq 10 is exactly zero while the mobility in that direction persists. As shown previously,[42] another procedure is then required to evaluate the transverse component of the diffusion tensor for probes diffusing in confined geometry

$$D_\alpha = \lim_{t\to\infty} \int_0^t \langle \vec{v}_\alpha(0)\vec{v}_\alpha(\tau)\rangle \, d\tau \qquad (11)$$

where the integrand of eq 11 stems for the corresponding component of the velocity autocorrelation function. Note that, for unlimited diffusion, the Green−Kubo relationship ensures the equivalence of both procedures.

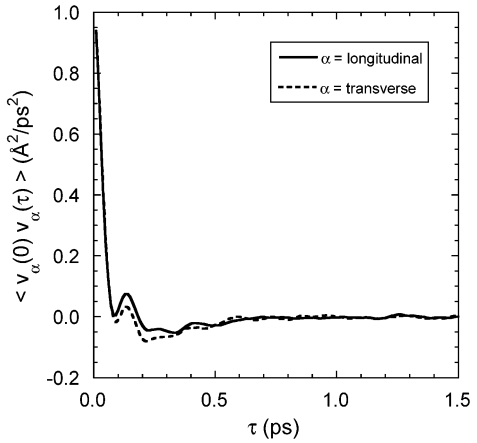

Figure 6. Longitudinal and transverse components of the velocity autocorrelation function of the confined water molecules calculated by molecular dynamics simulations.

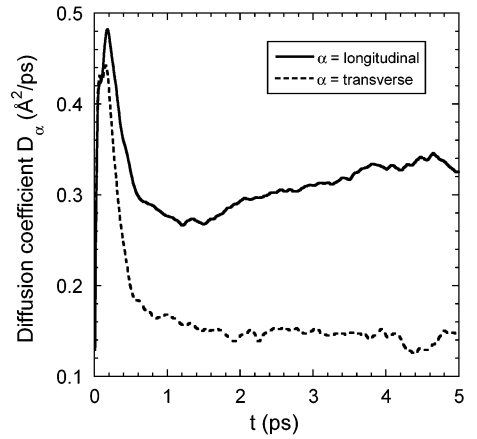

Figure 7. Longitudinal and transverse components of the tensor describing the water self-diffusion obtained from the integration of Figure 6 (see text).

Figure 6 displays the longitudinal (parallel to the clay surface) and transverse (perpendicular to the clay surface) components of the velocity autocorrelation function quantifying the mobility of the confined water molecules. Due to the fast decorrelation of both transverse and lateral motions, less than 2 ps are required to totally cancel these autocorrelation functions and the previous hypothesis of 50 independent trajectories is fully justified. The longitudinal and transverse components of the diffusion tensor are then evaluated by integrating these autocorrelation functions over 3 ps (see Figure 7), to avoid accumulation of noisy data. As shown in Figure 7, the longitudinal mobility of the water molecules near the clay surface [$(3.0 \pm 0.4) \times 10^{-9}$ m^2/s] is nearly the same as that of bulk water [$(3.3 \pm 0.3) \times 10^{-9}$ m^2/s for the TIP4P model[34]] and the transverse mobility of the confined water molecules is about half that value [$(1.5 \pm 0.2) \times 10^{-9}$ m^2/s]. As shown in Figure 8, the asymptotic slope of the longitudinal mean-squared displacement [$(3.7 \pm 0.4) \times 10^{-9}$ m^2/s] matches the value of the longitudinal mobility calculated from the integration of the velocity autocorrelation function.

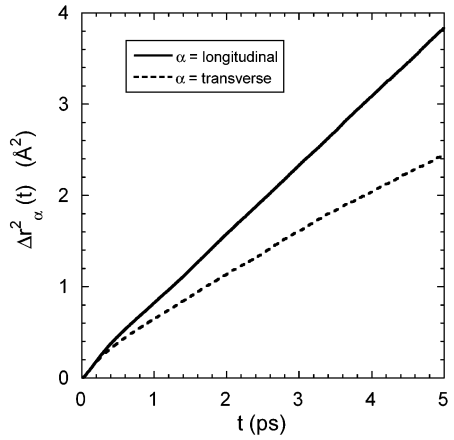

Figure 8. Longitudinal and transverse components of the water mean-squared displacement.

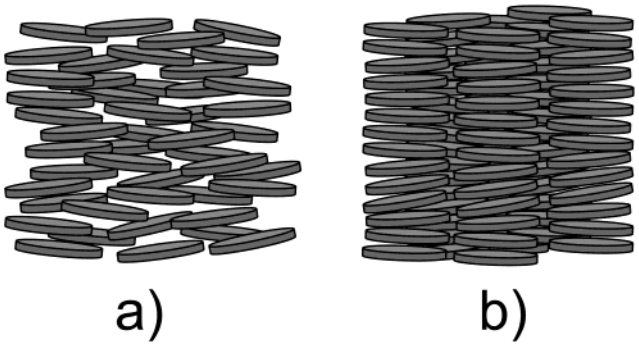

Figure 9. Schematic illustration of the (a) nematic and (b) columnar phases used for performing BD simulations of the water self-diffusion

(4) Brownian Dynamics Simulations. Brownian dynamics[23] (BD) was finally used to simulate the effective mobility of the water molecules within a dense nematic suspension of Laponite (45% w/w). To compare our numerical results with experimental data, we had to fill the gap between the time scale accessible by MD simulations (a few hundred picoseconds) and the experimental time scale (typically milliseconds). For that purpose, a collection (645) of rigid hard disks (diameter, 300; Å, thickness, 10 Å; and density, 2.7) were generated in a large simulation cell (0.14 μm width) with a predetermined nematic ordering (See Figure 9a) compatible with the information obtained by the line-shape analysis of our ^{23}Na NMR measurements.[10,30] The trajectories of 10000 diffusing probes are simulated by BD, using a time step (δt = 20 ps) 1 order of magnitude larger than the time scale (2 ps) required to fully decorrelate the water velocities (see Figure 6). Under such condition, the simple algorithm may be used[23]

$$\vec{x}_n(t+\delta t) = \vec{x}_n(t) + \vec{X}_n \tag{12a}$$

where $\vec{x}_n$ describes the coordinates of the center of mass of the nth water molecule and $\vec{X}_n$ a random Gaussian displacement, with first and second moments satisfying

$$\langle \vec{X}_n \rangle = 0 \tag{12b}$$

$$\langle (\vec{X}_n)^2_\alpha \rangle = 2(\overleftrightarrow{D}_n)_{\alpha\alpha}\delta t \tag{12c}$$

where $(\overleftrightarrow{D}_n)_{\alpha\beta} = \vec{e}_\alpha^T \overleftrightarrow{D}_n \vec{e}_\beta$. No specific clay/water interactions are described in this simplified model of aqueous clay dispersion. To take into account the local anisotropic mobility of the water molecules in the vicinity of the clay surface reported from our MD simulations (cf. Figures 6 and 7), the effective diffusion tensor of each probing water molecules in eq 12c is evaluated locally as a function of the transverse component of the separation between the water molecules and the rigid disks. As a consequence, when a water molecule is located inside a disk of diameter 300 Å and thickness 30 Å centered on a Laponite particle, its diffusion tensor is described locally by

$$(\overleftrightarrow{D}_n)_{xx} = (\overleftrightarrow{D}_n)_{yy} = 1.8 \times 10^{-9}\,\mathrm{m^2/s} \tag{13a}$$

$$(\overleftrightarrow{D}_n)_{zz} = 0.9 \times 10^{-9}\,\mathrm{m^2/s} \tag{13b}$$

where $(\vec{e}_x,\vec{e}_y,\vec{e}_z)$ is a local frame attached to the nearest disk with the $\vec{e}_z$ director perpendicular to the disk surface. In eq 13a,b, we have rescaled the local mobility of the condensed water molecules, as obtained by our previous MD simulations (see section II.C.3), since the TIP4P potential slightly overestimates the mobility of bulk water [2×10^{-9} m^2/s compared to 3.3×10^{-9} m^2/s (see above)]. Furthermore, to avoid discontinuities of the water mobility when a water molecule is located within a disk of diameter 300 Å and thickness 50 Å centered on a Laponite particle but excluded from any disk of the previous set, the tensor describing its mobility is defined locally by a linear interpolation between the limiting mobilities of bulk and confined water:

$$(\overleftrightarrow{D}_n)_{xx} = (\overleftrightarrow{D}_n)_{yy} = 1.8 \times 10^{-9}\,\mathrm{m^2/s} + \frac{Z-15}{10}[(\overleftrightarrow{D})^0_{\alpha\alpha} - 1.8 \times 10^{-9}\,\mathrm{m^2/s}] \tag{14a}$$

$$(\overleftrightarrow{D}_n)_{zz} = 0.9 \times 10^{-9}\,\mathrm{m^2/s} + \frac{Z-15}{10}[(\overleftrightarrow{D})^0_{\alpha\alpha} - 0.9 \times 10^{-9}\,\mathrm{m^2/s}] \tag{14b}$$

where Z is the distance between the water molecule and the equatorial plane of this remote Laponite disk. In this case, the distance Z satisfies the inequalities $15 \le |Z| \le 25$ Å. $(\overleftrightarrow{D})^0_{\alpha\alpha}$ describes the components of the isotropic diffusion tensor of bulk water (2×10^{-9} m^2/s). Finally when a water molecule is excluded from any of these remote disks, it diffuses freely as in bulk water.

The initial configuration of the 10000 diffusing probes is generated randomly by excluding the 645 Laponite disks. When the new position of the probe generated by our BD procedure falls inside a Laponite disk, the contact point is approximated by dividing the elementary trajectory into 10 equal segments and pure elastic collision is assumed. Since the maximum mobility of the water molecules corresponds to diffusion into bulk water, the time step of 20 ps is suitable to describe these clay/water collisions with the Laponite particle characterized by a thickness of 10 Å since the average displacement of the water molecules is smaller than 2.8 Å (see eq 12c).

The self-diffusion propagator[18] was used to analyze the mobility of the water molecules diffusing through the porous network limited by the Laponite particles. The self-diffusion propagator $P(\vec{r}|\vec{r}',\Delta)$ is defined as the density of probability to find at time Δ and position $\vec{r}'$a diffusing probe initially at a position $\vec{r}$

$$\Psi(\vec{r}',\Delta) = \int \Psi(\vec{r},0) P_s(\vec{r}|\vec{r}',\Delta)\mathrm{d}\vec{r} \tag{15}$$

where $\Psi(\vec{r},0)$ is the bulk density at equilibrium. For unrestricted diffusion within isotropic media, the self-diffusion propagator is Gaussian[18]

$$P(\vec{r}\,|\,\vec{r}\,',\Delta) = (4\pi D^0_{\alpha\alpha}\Delta)^{-3/2} \exp\left[-\frac{(\vec{r}-\vec{r}\,')^2}{4D^0_{\alpha\alpha}\Delta}\right] \quad (16)$$

From eq 16, one deduces the self-diffusion propagator describing the mobility along a single director[18] (noted $\vec{e}_z$)

$$P_z(Z|\Delta) = (4\pi D^0_{zz}\Delta)^{-1/2} \exp\left[-\frac{Z^2}{4D^0_{zz}\Delta}\right] \quad (17a)$$

whose Fourier transform is also Gaussian in the reciprocal q-space and is directly comparable with PGSE NMR measurements[18] (cf. eq 1)

$$E_z(q|\Delta) = \exp[-2\pi^2 q^2\langle Z^2\rangle] = \exp[-4\pi^2 q^2 D^0_{zz}\Delta] \quad (17b)$$

where $\langle Z^2\rangle$ is the mean-square displacement along the $\vec{e}_z$ director during the time delay Δ.

However, in the case of diffusion restricted by collisions at solid/liquid interfaces, the self-diffusion propagator and its Fourier transform are no longer Gaussian except in two limiting regimes:[18,43−50]

•at very short diffusion times, when the fraction of colliding probes remains negligible;

•at very large diffusion times, when the mobility of the probes is averaged over the whole structure of the solid interfaces, leading to an effective macroscopic mobility.

In addition to this classical picture, deviation from the simple Gaussian behavior is also expected to occur in our case at short diffusion time because of the supplementary heterogeneities introduced by the local variations and anisotropies of the tensor characterizing the mobility of the water molecules as a function of their separation from the Laponite disks. Since the calculated self-diffusion propagator results from the average of 10000 independent trajectories of the water molecules, one can estimate[51] its maximum uncertainty as about 0.01

(III) Results and Discussion

(A) Nematic Ordering of Dense Dispersions. The line shape detected by ^{23}Na (Figure 1a) or ^{7}Li (Figure 1b) NMR spectroscopy in the presence of dense Laponite aqueous dispersions (29−52% w/w) exhibits a large residual splitting, fingerprint of the macroscopic nematic ordering of the anisotropic particles.[10,30] The residual splitting detected by ^{23}Na NMR (28 kHz) agrees perfectly with the values calculated previously from GCMC simulations of the hydration of Laponite clay[24] neutralized by sodium counterions. It results from the anisotropy of the first hydration shell of the sodium counterion polarized by the electric charges of the clay particle. Of course the residual splitting detected with ^{23}Na NMR is larger than that reported by ^{7}Li NMR (390 Hz) in the presence of the same clay, because of its smaller quadrupolar moment (0.11×10^{-28} m^2 for ^{23}Na and 0.042×10^{-28} m^2 for ^{7}Li). However, the ratio of their quadrupolar moments ($Q_{Na}/Q_{Li} \sim 2.6$) cannot explain the ratio of the residual quadrupolar splitting ($\Delta\nu_{Q_{Na}}/\Delta\nu_{Q_{Li}} \sim 7.2$), and further GCMC simulations are required to analyze the hydration sphere of the Li^+ cation under the influence of the large electric field generated by the Laponite particle. One can note that the nematic director of the dense dispersions always coincides with the compression axis of the oedometer used to prepare these samples.

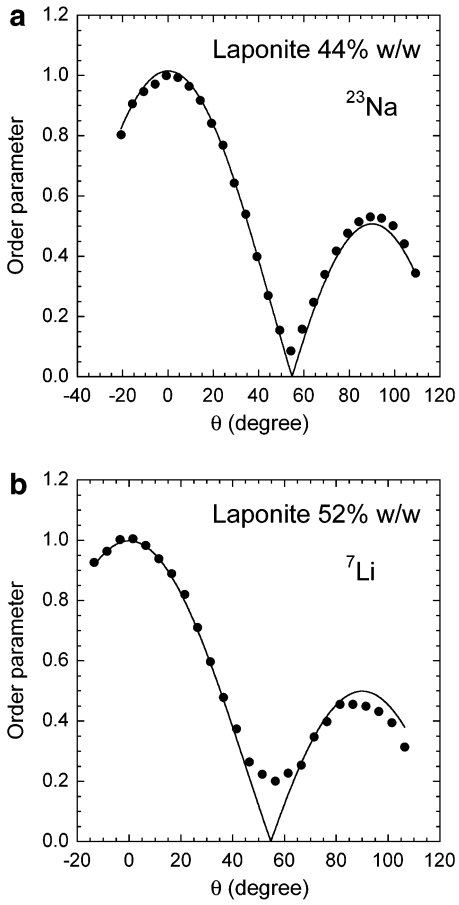

Figure 10. Order parameter deduced from the angular variation of the residual quadrupolar splitting displayed in Figure 1: (a) by ^{23}Na NMR spectroscopy and (b) by ^{7}Li NMR spectroscopy.

By analyzing the variation of the residual splitting as a function of the orientation of the nematic director in the static magnetic field[47] (see section II.B), it is possible to extract an order parameter[10] (Figure 10)

$$\Delta\nu_Q(\theta) = \left(\frac{3\cos^2(\theta)-1}{2}\right)\Delta\nu_Q^{MAX} \quad (18)$$

whose deviation from the perfect cancellation at the magic angle allows us to quantify the degree of local disorder[10,30] of the macroscopic nematic alignment.[52]

(B) ^{1}H PGSE NMR Diffusion Measurements. ^{1}H PGSE is a powerful tool to measure the mobility of the water molecule in confined media. Of course the proton mobility is higher than that of the water molecules since the first process implies only local motions of the protons through the network of hydrogen bonds while the second process requires macroscopic displacements of the water molecules. Furthermore ^{1}H NMR is sensitive to every spin population accessible to the hydrogen atoms. But in water at pH∼10, the relative abundance of the ionized populations is negligible ($[H^+] = 10^{-10}$ M, $[OH^-] = 10^{-4}$ M, and $[H_2O] = 55$ M) and they do not contribute significantly to the ^{1}H NMR signal.

By selecting six noncollinear directions[53] of the magnetic field gradient, we determine the various components of the tensor describing the mobility of the water molecules within these aqueous dispersions of clays. Figure 11 displays typical variations of the normalized echo amplitude (see eq 1 in section II.B). The evolution according to a Gaussian law (see also section II.C.4) clearly indicates that the PGSE measurements are

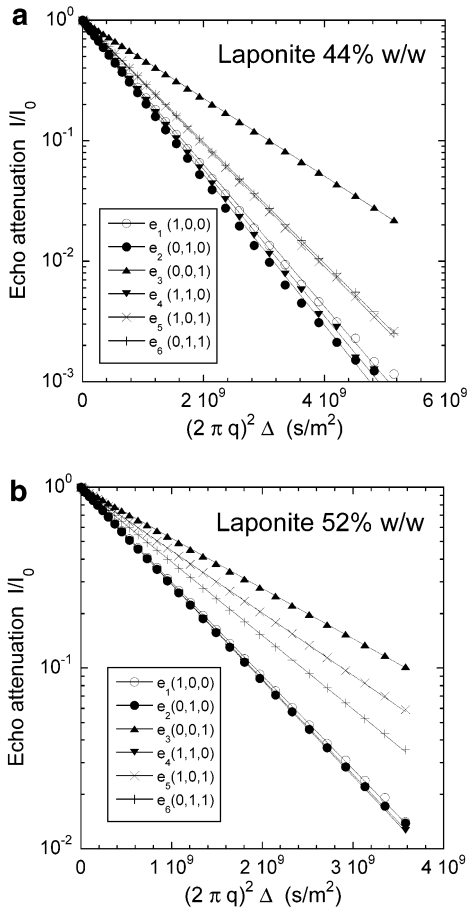

Figure 11. Measurement of the water mobility along six noncollinear directors used to extract the eigenvalues and eigenvectors of the tensor describing the water self-diffusion within dense Laponite dispersions: (a) (44% w/w) neutralized by the sodium counterions and (b) (52% w/w) neutralized by the lithium counterions.

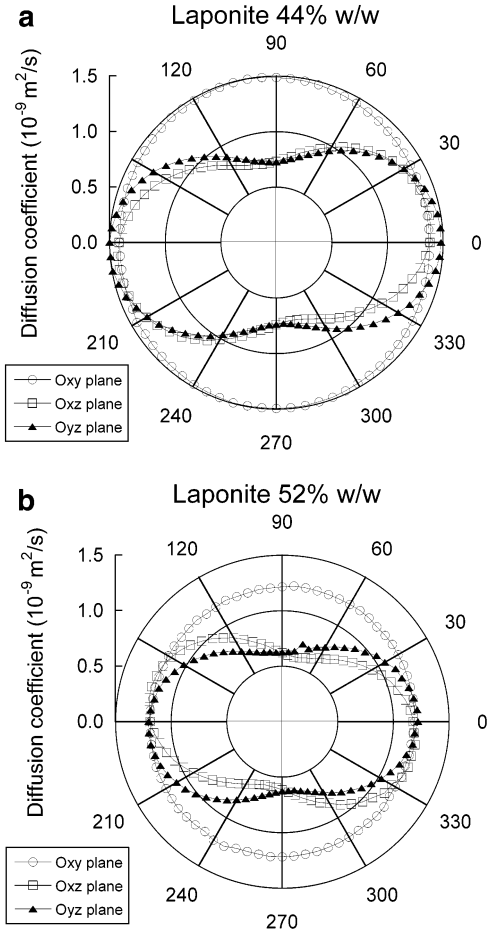

Figure 12. Variation of the water mobility along a director varying inside each of the three planes defined by two of the previously determined eigenvectors of the self-diffusion tensor of dense Laponite dispersions: (a) (44% w/w) neutralized by the sodium counterions and (b) (52% w/w) neutralized by the lithium counterions.

sensitive to the macroscopic effective mobility of the water molecules averaged over the whole sample. From elementary algebra, the eigenvalues of the self-diffusion tensor and the corresponding principal axis are extracted.

To further illustrate the anisotropy of the water self-diffusion within the dense nematic dispersions we have also analyzed the influence on the water mobility of the gradual variation of the direction of the applied field gradient within the three planes defined by two of the previously identified principal axes of the diffusion tensor (noted $\vec{e}_\alpha$ and $\vec{e}_\beta$). The measured diffusion coefficient (see Figure 12) varies according to

$$D_{\text{meas}}(\theta) = \vec{e}_g^{\,T}\overleftrightarrow{D}\vec{e}_g = D_{\alpha\alpha}\cos^2(\theta) + D_{\beta\beta}\sin^2(\theta) \quad (19)$$

where θ is the angle between $\vec{e}_\alpha$ and $\vec{e}_g$, and $D_{\alpha\alpha}$ and $D_{\beta\beta}$ are the eigenvalues of the diffusion tensor corresponding to the principal directors $\vec{e}_\alpha$ and $\vec{e}_\beta$.

The anisotropy of the water self-diffusion tensor further confirms the detection of a nematic ordering (see Table 4) which propagates through the whole sample. As an example, one notes a perfect correlation between the maximum amplitude of the residual quadrupolar splitting detected by ^{23}Na NMR and the tortuosity determined from the normalized apparent self-diffusion of the water molecules ($\tau_\alpha = D^0_{\alpha\alpha}/D^{\text{exp}}_{\alpha\alpha}$), where $D^0_{\alpha\alpha}$ is the water self-diffusion in bulk water. As expected, the tortuosity characterizing the water transverse motion (perpendicular to the clay surfaces) is much larger than the tortuosity characterizing the longitudinal motion (parallel to the clay surface) due to the aspect ratio of the Laponite particles. The cross-section of the basal surfaces of the Laponite disks (diameter 300 Å) is indeed larger than their lateral cross-section (thickness 10 Å). As a consequence the director corresponding to the largest tortuosity coincides with the nematic director detected by ^{23}Na and ^{7}Li NMR (see Table 4).

TABLE 4: Results from the ^{1}H, ^{7}Li, and ^{23}Na NMR Experiments[a]

sample	$D_{\text{trans}}/D^0_{\alpha\alpha}$	$D_{\text{long}}/D^0_{\alpha\alpha}$	τ_{trans}	τ_{long}	$\Delta\nu_Q^{\text{MAX}}$ (kHz)
water	1	1	1	1	
3% w/w	0.93 ± 0.03	0.95 ± 0.03	1.07	1.05	0 (^{23}Na)
29% w/w	0.53 ± 0.03	0.75 ± 0.03	1.90	1.33	16 ± 2 (^{23}Na)
32% w/w	0.45 ± 0.03	0.65 ± 0.03	2.20	1.55	16 ± 2 (^{23}Na)
44% w/w	0.37 ± 0.03	0.75 ± 0.03	2.71	1.33	22 ± 2 (^{23}Na)
45% w/w	0.37 ± 0.03	0.76 ± 0.03	2.69	1.32	28 ± 2 (^{23}Na)
52% w/w*	0.32 ± 0.03	0.63 ± 0.03	3.16	1.58	0.39 ± 0.05 (^{7}Li)

[a] All measurements were performed with dispersions of Laponite clay neutralized by sodium counterions except in the last case (52% w/w*) which corresponds to Laponite neutralized by lithium counterions. The self-diffusion coefficient of bulk water (1.92×10^{-9} m^2/s) was also measured by ^{1}H PGSE NMR.

(C) Multiscale Modeling of Water Diffusion. As detailed in section II.D.4, we used BD simulations, with an effective local mobility of the water molecules, to produce numerical data directly comparable with the macroscopic experimental diffusion measurements by using a model of the clay/water interface based on a quantum description of the clay/water interactions at an atomic scale and preventing the introduction of artificial or

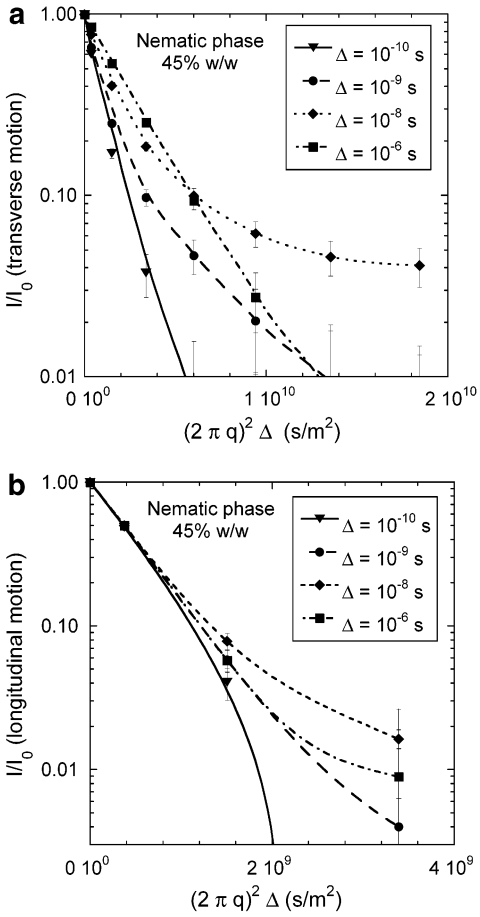

Figure 13. Self-diffusion propagators analyzing the transverse (a) and longitudinal (b) mobility of the water molecules derived by BD simulations of the water trajectories within a pure nematic phase (45% w/w) of rigids platelets (diameter 300 Å).

arbitrary parameters. Our first model of clay dispersions is a pure nematic dispersion of 645 rigid disks (diameter, 300 Å; thickness, 10 Å; and density, 2.7) distributed in a large simulation cell (width 1.4×10^{-7} m) without any positional order and corresponding to fully exfoliated Laponite particles (cf. Figure 9a). We focus on the Fourier transform of the self-diffusion propagator (cf. eq 17b) because it is directly comparable with our experimental ^{1}H PGSE NMR measurements (cf. eq 1). The time delays Δ used in these dynamical simulations are 10^{-10}, 10^{-9}, 10^{-8}, 3×10^{-8}, 6×10^{-8}, 10^{-7}, 3×10^{-7}, 6×10^{-7}, and 10^{-6} s.

Two limiting dynamical regimes are clearly identified on the water transverse diffusion (cf. Figure 13a) corresponding to Gaussian behaviors at short ($\Delta = 10^{-10}$ s) and large ($\Delta \geq 3 \times 10^{-7}$ s) diffusion times. This result at large diffusion time proves that the time scale sampled by these BD simulations is large enough to fully average the dynamical properties of the water molecules over the spatial structure of the simulated clay suspension. As a consequence, if no heterogeneity of the clay density occurs at a length scale larger than the size of the simulation cell, the data calculated at a diffusion delay (Δ) larger than 3×10^{-7} s may be compared with the macroscopic experimental NMR measurements. The size of the representative elementary volume corresponding to this asymptotic regime is estimated from the relationship $L \approx \sqrt{2\Delta D^0_{\alpha\alpha}} \approx 3.5 \times 10^{-8}$ m, i.e., the order of magnitude of the Laponite diameter. The apparent transverse mobility corresponding to these two limiting regimes [(1.2 and 0.42) $\times 10^{-9}$ m^2/s, respectively, for the short and large diffusion times] are detailed in Table 5.

TABLE 5: Apparent Transverse Mobility of the Water Molecules Obtained by BD Simulations

diffusion time	nematic phase	columnar phase
10^{-10} s	1.2×10^{-9} m^2/s	1.3×10^{-9} m^2/s
10^{-9} s	0.98×10^{-9} m^2/s	0.94×10^{-9} m^2/s
10^{-8} s	0.63×10^{-9} m^2/s	0.76×10^{-9} m^2/s
3×10^{-8} s	0.50×10^{-9} m^2/s	0.82×10^{-9} m^2/s
6×10^{-8} s	0.47×10^{-9} m^2/s	0.88×10^{-9} m^2/s
10^{-7} s	0.44×10^{-9} m^2/s	0.94×10^{-9} m^2/s
3×10^{-7} s	0.40×10^{-9} m^2/s	1.05×10^{-9} m^2/s
6×10^{-7} s	0.42×10^{-9} m^2/s	1.13×10^{-9} m^2/s
10^{-6} s	0.40×10^{-9} m^2/s	1.12×10^{-9} m^2/s

This result quantifies the decrease of the effective water mobility induced by the numerous collisions occurring during its diffusion through the porous network limited by the clay particles.

Large deviations from the limiting Gaussian regime are detected in the intermediate diffusion times (see Figure 13a) and are the fingerprints of diffusion within confined geometries.[18,54] Nevertheless, quantitative information on the water mobility $\nu_\alpha(\Delta)$ on the diffusion time scale Δ may be extracted from the limiting slope displayed in Figure 13:

$$\nu_\alpha(\Delta) = -\lim_{q\to 0}\left(\frac{\ln E_\alpha(q,\Delta)}{4\pi^2 q^2 \Delta}\right) \tag{20a}$$

where the macroscopic component of the self-diffusion tensor is defined by

$$D_{\alpha\alpha} = \lim_{\Delta\to\infty} \nu_\alpha(\Delta) \tag{20b}$$

The water transverse mobilities evaluated at intermediate time scales ($10^{-10} < \Delta < 3 \times 10^{-7}$ s) are also displayed in Table 5. They exhibit a continuous decrease of the transverse apparent mobility of the water molecules before it reaches its asymptotic value [$D_{trans} = (0.42 \pm 0.04) \times 10^{-9}$ m^2/s], which is significantly smaller than the experimental value [$D_{trans} = (0.73 \pm 0.02) \times 10^{-9}$ m^2/s; see Table 4].

By contrast with the behavior reported for the transverse motion, the longitudinal motion of the water molecules does not exhibit large deviations from the Gaussian regime (see Figure 13b), because the lateral cross-section of the Laponite particle is small and because the longitudinal mobility of the water molecules near the clay surface (cf. eq 13a) is very similar to that of bulk water. One also notes that the simulated longitudinal component of the self-diffusion tensor [$(1.80 \pm 0.04) \times 10^{-9}$ m^2/s] exceeds the experimental value [$D_{long} = (1.36 \pm 0.02) \times 10^{-9}$ m^2/s; see Table 4].

To check for the influence of the structure of the clay dispersion on the apparent mobility of the water molecules, we have generated, in the same cubic simulation cell (width, 0.14 μm), a columnar phase obtained by generating randomly 15 parallel and nonoverlapping columns, each resulting from the stack of 43 rigid disks (Figure 9b). The position of the Laponite particles within these columns is obtained by applying a small translation (maximum amplitude 5 Å) to a purely periodic crystal (with a period of 32.6 Å along the director of the columns). As previously, the orientation of the rigid disks within these columns is selected to reproduce the experimental nematic ordering detected by ^{23}Na NMR.

Large deviations from the limiting Gaussian regime are again reported for the transverse mobility of the water molecules in the intermediate time scale ($10^{-10} < \Delta < 3 \times 10^{-7}$ s; Figure 14a) while Gaussian behavior is detected at short ($\Delta = 10^{-10}$ s) and large ($\Delta \geq 3 \times 10^{-7}$ s) diffusion times. Here also, the

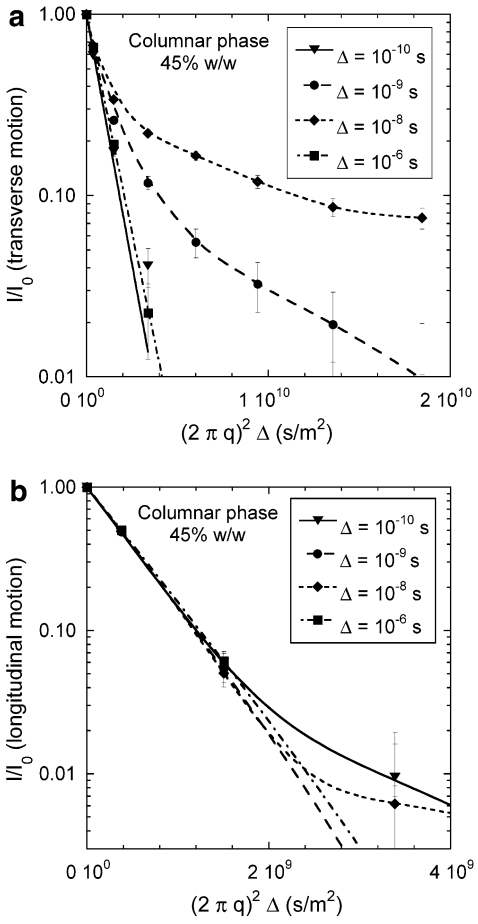

Figure 14. Same as Figure 13 for a columnar phase.

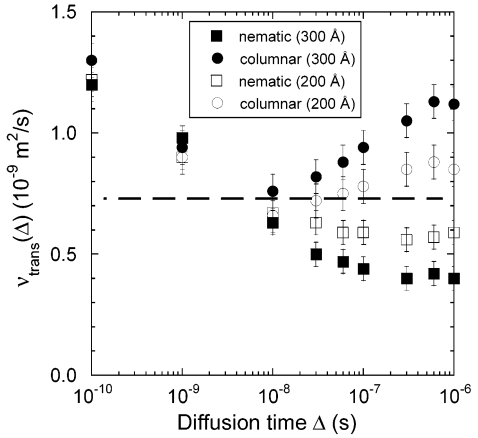

Figure 15. Variation of the water transverse mobility $\nu_{trans}(\Delta)$ as a function of the diffusion time Δ; the horizontal line corresponds to the water asymptotic mobility measured by ^{1}H PGSE NMR.

longitudinal diffusion is almost Gaussian at every diffusion time (Figure 14b), with an apparent longitudinal component of the self-diffusion tensor [$(1.88 \pm 0.04) \times 10^{-9}$ m^2/s] similar to the value estimated for the nematic phase. The main difference is reported for the transverse mobility whose variation is non-monotonic (see Table 5 and Figure 15): starting from $(1.30 \pm 0.04) \times 10^{-9}$ m^2/s it reaches a minimum value $(0.76 \pm 0.04) \times 10^{-9}$ m^2/s after a diffusion time of 10^{-8} s and then increases back to $(1.13 \pm 0.04) \times 10^{-9}$ m^2/s at diffusion time larger than 3×10^{-7} s. The long-time limiting transverse mobility calculated for this columnar phase is now larger than the experimental value [$D_{trans} = (0.73 \pm 0.02) \times 10^{-9}$ m^2/s, see Table 4].

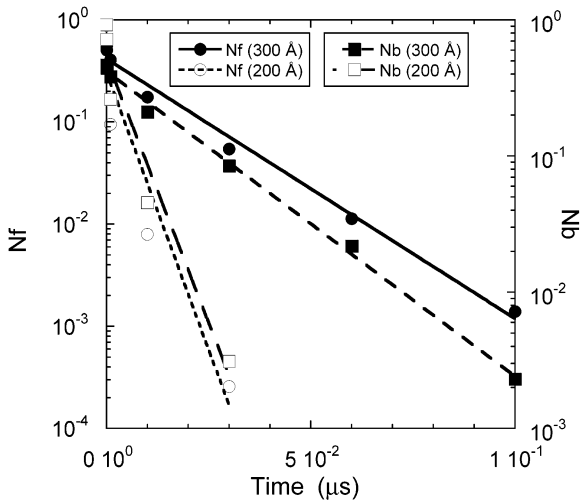

Figure 16. Analysis of the average residence time of the water molecules within the free and confined environments within the columnar phases resulting from the stacking of rigid disks of diameter 200 or 300 Å.

The origin of this non-monotonic variation of the transverse mobility is difficult to assess. Clearly, the apparent transverse mobility of the water molecules in this columnar phase results from a mixture of two limiting behaviors corresponding respectively to free water, located between the columns and with a high mobility, and confined water, localized inside the columns and with a lower mobility. However, the long-time asymptotic value of the water mobility [$(1.05 \pm 0.04) \times 10^{-9}$ m^2/s in these simulations] drastically differs from the value estimated by averaging the water mobility characteristic of the free and condensed environments

$$\langle D \rangle = p_F D_F + p_{cond} D_{cond} = [(0.53)\times(2) + (0.47)\times(0.9)] \times 10^{-9}\,\mathrm{m^2/s} = 1.4810^{-9}\,\mathrm{m^2/s} \quad (21)$$

since the numerous collisions of the water molecules on the clay surfaces restrict the extent of their diffusion space, generating the apparent tortuosity of the porous medium. To better characterize the time scale associated with the exchange between both environments, we have also determined the mean residence time of the water molecules from the decrease of the fraction of water molecules initially located in these environments (see Figure 16). The fits to a simple exponential law give residence times of 1.7×10^{-8} and 1.9×10^{-8} s for free and confined water, respectively. That time scale corresponds roughly to the minimum of the apparent transverse mobility of the water molecules within the columnar phase (see Table 5). As expected, the limiting Gaussian behavior is reached after a diffusion time larger than 3×10^{-7} s, when both environments are totally mixed. Of course a somewhat different behavior will be observed for another distribution of the Laponite disks within the columnar phase, by increasing the number of columns and thus decreasing their separation and the average residence time of the water molecules in the free environment. A lower transverse mobility of the water molecules at long diffusion time will emerge from this new geometry, since it corresponds to a decrease of the transverse cross-section of the free space located between the columns.

To further probe the influence of the shape of the clay particles and of the structure of the dispersion on the effective mobility of the water molecules, we have also performed BD simulations with smaller rigid disks (diameter of 200 Å), either distributed randomly within a nematic phase or organized within

a columnar phase. To maintain the density of the dispersion (45% w/w), both systems contain 1440 particles within the same simulation cell (width, 0.14 μm). The new columnar phase results from the stack of 36 parallel disks within 40 columns with an average separation of 38.9 Å between the elementary disks. The results obtained with these smaller disks are qualitatively similar to those displayed in Figures 13 and 14 and summarized in Figure 15. The propagators describing the longitudinal motion are almost Gaussian, with the same overestimate of the experimental longitudinal mobility. By contrast, the transverse mobility is more sensitive to the size of the particles: Figure 15 clearly exhibits both an increase of the long-time mobility within the nematic phase and a decrease within the columnar phase. As shown in Figure 16, the time scale characterizing the exchange between the free and confined water molecules is reduced by a factor three because both the surface of the disks and the section of the empty space between the columns are smaller.

The main difference between molecular liquid crystals and these clay dispersions is the large size heterogeneity of the particles. To probe the influence of such heterogeneities, we have performed BD simulations for two disk diameters (200 and 300 Å) corresponding to the upper and lower size limits expected to occur within the synthetic Laponite clay. As an example, such size heterogeneities may be responsible for some microsegregation of the Laponite dispersions, with coexistence of ordered and disordered microdomains. However, since the orientational ordering used to model the platelets distribution is determined a priori in order to reproduce the macroscopic nematic ordering detected by ^{23}Na NMR, we may infer that the dynamical behavior of the real heterogeneous sample is included between the two limiting behaviors predicted by our BD simulations. As a consequence, the data displayed in Figure 15 clearly demonstrate that the influence on the water mobility of the size heterogeneity of the Laponite particle is reduced (less than 20%) and does not affect the conclusions of our dynamical study.

(IV) Limitations and Perspectives

By using numerical simulations of Brownian dynamics, we obtained semiquantitative agreement between the measured and calculated mobility of the water molecules within dense clay dispersions. Of course the agreement with the experimental data could be improved, for example, by introducing a supplementary parameter describing the average residence time[24] of the water molecules adsorbed at the clay surface. However, we preferred to use these BD simulations to predict the macroscopic dynamical properties of the solvent molecules without introducing any artificial or fitted parameters, but using information on the local mobility of the water molecules imported from preliminary statistical (MD, GCMC) and quantum (MINDO) studies performed on a smaller scale. Nevertheless, the major deficiency of our BD simulations concerns the lack of a detailed description of the interaction of the water molecules with the lateral surface of the clay particle, since only elastic collisions were considered here. Since our quantum calculation and GCMC and MD simulations consider only the interaction of the water molecules with the basal surface of the clay particles, edge effects are not well reproduced in that study. Obviously, in dilute isotropic dispersions, edge effects are expected to be negligible because of the large anisotropy of the particle, leading to large difference between the longitudinal and transverse cross-sections of the clay particle. But in concentrated regime and nematic dispersions, the diffusion in the direction parallel to the clay surface may become highly sensitive to the interaction of the water molecules with the lateral surfaces of the clay. Indeed the leading term is now the ratio between the thickness of the clay particle (10 Å) and the separation between the clay platelets. As an example, for a clay density of 50% w/w, that separation is of the order of 40 Å. As a consequence, edge effects cannot be totally neglected. This deficiency is perhaps responsible for the largest disagreement of the prediction of the longitudinal component of the mobility of the water molecules, by comparison with the transverse mobility. Another limitation concerns the validity of the empirical TIP4P model, initially devised to model thermodynamical properties of bulk water, and applied here to describe the water/water and ion/water interactions in confined geometry. As a consequence, this study must be considered as a first approach, leading only to a semiquantitative prediction of the dynamical behavior of the water molecules confined between clay particles by bridging the gap between the time scale accessible by MD (nanosecond) and that corresponding to macroscopic measurements. A more self-consistent and satisfactory approach will result from the direct use of DFT quantum calculations[55,56] to analyze the local mobility of the water molecules near the clay surface.

This study, performed on an ideal system (synthetic Laponite clays), also demonstrated the great influence of the structure of the colloidal dispersion and the shape of the particles on the effective tortuosity characterizing the mobility of the solvent molecules diffusing trough the porous network limited by the solid particles. Further investigations will be performed, both experimentally and numerically, applying the same procedure to characterize the mobility of the water molecules and ionic probe diffusing in aqueous dispersions of natural clays, such as the bentonite, used for storing of nuclear waste. To detect experimentally, i.e., on the time scale of a few milliseconds, deviations from the asymptotic Gaussian regime, it will be necessary to increase at least by 2 orders of magnitude the size of the elementary particles which restrict the diffusion space of the solvent molecules, since the time scale necessary to average the dynamical behavior within such samples will increase by 4 orders of magnitude.

(V) Conclusions

By analyzing the line shape detected by nuclear magnetic resonance of quadrupolar nuclei (^{7}Li and ^{23}Na) in the presence of dense aqueous dispersions of clays, we detected a nematic ordering of the clay particles. This ordering is confirmed by ^{1}H pulsed field gradient nuclear magnetic resonance measurements of the anisotropy of the tensor describing the water self-diffusion. A multiscale analysis of the solvent mobility within a model of clay dispersions is used to semiquantitatively describe these experimental data, by importing into numerical simulations of Brownian dynamics structural and dynamical information obtained from a double quantum (MINDO) and statistical (grand canonical Monte Carlo simulations, simulations of molecular dynamics) description of the clay/water interface.

Acknowledgment. We cordially thank Drs. P. Levitz, S. Rodts, J. Puibasset, and R. Setton for helpful discussions. NMR spectrometers were purchased thanks to grants from Région Centre (France). Quantum calculations were performed on workstations at IDRIS (CNRS, Orsay, France). Monte Carlo, MD, and DB simulations were performed locally on workstations purchased thanks to grant from Région Centre (France).

References and Notes

(1) Ramsay, J. D. F.; Lindner, P. *J. Chem. Soc., Faraday Trans.* **1993**, *89*, 4207.
(2) Gabriel, J. C. P.; Sanchez, C.; Davidson, P. *J. Phys. Chem.* **1996**, *100*, 11139.
(3) Pignon, F.; Magnin, A.; Piau, J. M.; Cabane, B.; Lindner, P.; Diat, O. *Phys. Rev. E* **1997**, *56*, 3281.
(4) Kroon, M.; Vos, W. L.; Wegdam, G. H. *Phys. Rev. E* **1998**, *57*, 1962.
(5) Bonn, D.; Tanaka, H.; Wegdam, G.; Kellay, H.; Meunier, J. *Europhys. Lett.* **1998**, *45*, 52.
(6) Saunders, J. M.; Goodwin, J. W.; Richardson, R. M.; Vincent, B. *J. Phys. Chem. B* **1999**, *103*, 9211.
(7) Nicolai, T.; Cocard, S. *Langmuir* **2000**, *16*, 8189.
(8) Levitz, P.; Lécolier, E.; Mourchid, A.; Delville, A.; Lyonnard, S. *Europhys. Lett.* **2000**, *49*, 672.
(9) Bellon, L.; Ciliberto, S.; Laroche, C. *Europhys. Lett.* **2001**, *53*, 511.
(10) Porion, P.; Rodts, S.; Al Mukhtar, M.; Faugère, A. M.; Delville, A. *Phys. Rev. Lett.* **2001**, *87*, 208302.
(11) Aubry, T.; Bossard, F.; Moan, M. *Langmuir* **2002**, *18*, 155.
(12) Cousin, F.; Cabuil, V.; Levitz, P. *Langmuir* **2002**, *18*, 1466.
(13) Bakk, A.; Fossum, J. O.; da Silva, G. J.; Adland, H. M.; Mikkelsen, A.; Elgsaeter, A. *Phys. Rev. E* **2002**, *65*, 21407.
(14) Ramsay, J. D. F. *J. Colloid Interface Sci.* **1986**, *109*, 441.
(15) Mourchid, A.; Delville, A.; Lambard, J.; Lécolier, E.; Levitz, P. *Langmuir* **1995**, *11*, 1942.
(16) Fredrickson, G. H.; Bicerano, J. *J. Chem. Phys.* **1999**, *110*, 2181.
(17) Stejskal, E. O.; Tanner, J. E. *J. Chem. Phys.* **1965**, *42*, 288.
(18) Callaghan, P. T. *Principles of Nuclear Magnetic Resonance Microscopy*; Clarendon Press: Oxford, 1991.
(19) Adams, D. J. *Mol. Phys.* **1974**, *5*, 1241.
(20) Nicholson, D.; Parsonage, N. G.; Rowley, L. A. *Mol. Phys.* **1981**, *44*, 629.
(21) Allen, M. P.; Tildesley, D. J. *Computer Simulation of Liquids*; Clarendon Press: Oxford, 1994.
(22) Fincham, D. *Mol. Simul.* **1992**, *8*, 165.
(23) Van Gunsteren, W. F.; Berendsen, H. J. C.; Rullmann, J. A. C. *Mol. Phys.* **1981**, *44*, 69.
(24) Porion, P.; Faugère, M. P.; Lécolier, E.; Gherardi, B.; Delville, A. *J. Phys. Chem. B* **1998**, *102*, 3477.
(25) Chang, F. R. Ch.; Skipper, N. T.; Sposito, G. *Langmuir* **1998**, *14*, 1201.
(26) Leote de Carvalho, R. J. F.; Skipper, N. T. *J. Chem. Phys.* **2001**, *114*, 3727.
(27) Marry, V.; Turq, P.; Cartailler, T.; Levesque, D. *J. Chem. Phys.* **2002**, *117*, 3454.
(28) Thompson, D. W.; Butterworth, J. T. *J. Colloid Interface Sci.* **1992**, *151*, 236.
(29) Mourchid, A.; Levitz, P. *Phys. Rev. E* **1998**, *57*, R4887.
(30) Porion, P.; Al Mukhtar, M.; Meyer, S.; Faugère, A. M.; van der Maarel, J. R. C.; Delville A. *J. Phys. Chem. B* **2001**, *105*, 10505.
(31) Delville, A. *Langmuir* **1991**, *7*, 547.
(32) Pellenq, R. J. M.; Nicholson, D. *J. Phys. Chem.* **1994**, *98*, 13339.
(33) Pellenq, R. J. M.; Nicholson, D. *Mol. Phys.* **1998**, *3*, 549.
(34) Jorgensen, W. L. *J. Chem. Phys.* **1982**, *77*, 4156.
(35) Bounds, D. G. *Mol. Phys.* **1985**, *54*, 1335.
(36) Heyes, D. M. *Phys. Rev. B* **1994**, *49*, 755.
(37) Hummer, G. *Chem. Phys. Lett.* **1995**, *235*, 297.
(38) Delville, A.; Sokolowski, S. *J. Phys. Chem.* **1993**, *97*, 6261.
(39) Delville, A. *J. Phys. Chem.* **1995**, *99*, 2033.
(40) Evans, D. J.; Murad, S. *Mol. Phys.* **1977**, *34*, 327.
(41) Berendsen, H. J. C.; Postma, J. P. M.; van Gunsteren, W. F.; DiNola, A.; Haak, J. R. *J. Chem. Phys.* **1984**, *81*, 3684.
(42) Schoen, M.; Cushman, J. H.; Diestler, D. J.; Rhykerd, C. L., Jr. *J. Chem. Phys.* **1988**, *88*, 1394.
(43) Callaghan, P. T.; Coy, A.; MacGowan, D.; Packer, K. J.; Zelaya, F. O. *Nature* **1991**, *351*, 467.
(44) Mitra, P. P.; Sen, P. N.; Schwartz, L. M.; Le Doussal, P. *Phys. Rev. Lett.* **1992**, *68*, 3555.
(45) Sen, P. N.; Hürlimann, M. D.; de Swiet, Th. M. *Phys. Rev. B* **1995**, *51*, 601.
(46) Bergman, D. J.; Dunn, K. J.; Schwartz, L. M.; Mitra, P. P. *Phys. Rev. E* **1995**, *51*, 3393.
(47) Nakashima, Y.; Mitsumori, F.; Nakashima, S.; Takahashi, M. *Appl. Clay Sci.* **1999**, *14*, 59.
(48) Griffith, P. C.; Stilbs, P.; Howe, A. M.; Cosgrove, T. *Langmuir* **1996**, *12*, 2884.
(49) Johannesson, H.; Furo, I.; Halle, B. *Phys. Rev. E* **1996**, *53*, 4904.
(50) Holz, M.; Heil, S. R.; Sacco, A. *Phys. Chem. Chem. Phys.* **2000**, *2*, 4740.
(51) Duh, A.; Mohoric, A.; Stepisnik, J. *J. Magn. Res.* **2001**, *148*, 257.
(52) Zghal, M.; Auroy, P.; Deloche, B. *Phys. Rev. Lett.* **1995**, *75*, 2140.
(53) Basser, P. J.; Mattiello, J.; LeBihan, D. *J. Magn. Res. B* **1994**, *103*, 247.
(54) Callaghan, P. T.; Soderman, O. *J. Phys. Chem.* **1983**, *87*, 1737.
(55) Odelius, M.; Bernasconi, M.; Parrinello, M. *Phys. Rev. Lett.* **1997**, *78*, 2855.
(56) Marx, D.; Hutter, J. *Ab Initio Molecular Dynamics: Theory and Implementation* in *Modern Methods and Algorithm of Quantum Chemistry*; Grotendorst, J., Ed.; NIC Series 1; Forschungszentrum Jülich: 2000, p 301.
(57) Puibasset, J.; Pellenq, R. J. M. *J. Chem. Phys.* **2003**, *118*, 5613.
(58) Fripiat, J.; Cases, J.; François, M.; Letellier, M. *J. Colloid Interface Sci.* **1982**, *89*, 378.
(59) Israelachvili, J. N.; Pashley, R. M. *Nature* **1983**, *306*, 249.
(60) Chavez-Paez, M.; van Workum, K.; de Pablo, L.; de Pablo, J. J. *J. Chem. Phys.* **2001**, *114*, 1405.
(61) Ichikawa, Y.; Kawamura, K.; Nakano, M.; Kitayama, K.; Seiki, T.; Theramast, N. *Eng. Geol.* **2001**, *60*, 127.